CHAPTER IV

BEHAVIOR OF REINFORCED CONCRETE COLUMNS AND PLANE FRAMES

4.1 Introduction

The capability of the proposed confinement and reinforcement buckling models is assessed by comparing the analytical envelope moment-curvature relationships of sample reinforced concrete columns with experimental results from cyclic load tests.

4.1.1 Procedure for Determining Moment-curvature Relationship

To determine the moment-curvature curves associated with different axial load levels, it is convenient to divide the section into a number of discrete laminae, each being parallel to the neutral axis as shown in Figure 4.1(a). Each lamina then contains a quantity of core concrete and cover concrete. Assuming the plane section remains plane during deformation, as shown in Figure 4.1 (b), the average strain in each concrete lamina is then calculated. The stresses in the core concrete and cover concrete are then determined from the stress-strain relationships of the confined and unconfined concrete, respectively. The strains and stresses in the longitudinal reinforcing bars can also be similarly computed.

The theoretical moment-curvature relationship for a given axial load level can be determined by incrementing the concrete strain in the extreme compression fiber, ε_{cm}. For a given set of axial force, P, and moment, M, the neutral axis depth, d', is found from the condition that the following equilibrium equations be satisfied:

$$P = \sum_{i=1}^{nc} \left(\sigma_{uci} A_{uci} + \sigma_{ci} A_{ci}\right) + \sum_{i=1}^{nb} \sigma_{si} A_{si} \tag{4.1}$$

$$M = \sum_{i=1}^{nc} \left(\sigma_{uci} A_{uci} + \sigma_{ci} A_{ci}\right) d_{ci} + \sum_{i=1}^{nb} \sigma_{si} A_{si} d_{si} - P\frac{B}{2} \tag{4.2}$$

where σ_{uci}, σ_{ci} and σ_{si} are, respectively, the unconfined compressive stress, confined compressive stress of the i^{th} lamina and stress in the i^{th} layer of the longitudinal reinforcement; A_{uci}, A_{ci}, and A_{si} are, respectively, the area of cover concrete, core concrete in the i^{th} lamina and the area of longitudinal reinforcement in the i_{th} layer; nc denotes the numbers of concrete lamina and nb the number of layers of longitudinal reinforcement; and d_{ci} and d_{si} are the distances of the centroid of the i^{th} lamina of concrete and the i^{th} layer of the longitudinal reinforcement from the extreme compression fiber, respectively. The curvature, ϕ, corresponding to the moment M is given by

$$\phi = \frac{\varepsilon_{cm}}{d'} \tag{4.3}$$

In this study, the proposed confinement model described in Chapter II is used for concrete core. The stress-strain relationship including buckling [Dhakal (2000)] is used to model the longitudinal reinforcements under compressive loading. For unconfined concrete, the stress-strain relationship proposed by Mander et al. (1988) is applied for the concrete cover. A small computer program was developed to determine the analytical moment-curvature relationships.

4.1.2 Comparison of Analytical and Experimental Envelope Moment-curvature Relationships

Figures 4.2-4.5 show the envelope moment-curvature relationships for the columns tested at Chulalongkorn University by Lukkunaprasit and Sittipunt (2003) while Figures 4.6-4.7 present the moment-curvature relationships for those tested by Sheikh and Khoury (1993). The analytical stress-strain relationships of the longitudinal bars under compressive strains are shown in Figure 4.8. The details for the columns considered are given in Tables 4.1 and 4.2. It can be seen from those figures that the peak moments are satisfactorily predicted with a maximum discrepancy of about 11%. It is also obvious from Figures 4.2-4.5 that the buckling of longitudinal reinforcements has significant effect on the load-carrying capacity of the columns. For the columns tested at Chulalongkorn University by Lukkunaprasit and Sittipunt (2003), good predictions of the overall moment-curvature curves are observed. However, for the columns tested by Sheikh and Khoury (1993), the proposed procedure cannot predict the descending

branches of the moment-curvature relationships. It is observed that the major differences between the columns tested by Lukkunaprasit and Sittipunt (2003) and those tested by Sheikh and Khoury (1993) are the amount of confinement and the arrangement of the transverse steels. The volumetric ratio of the transverse steel, ρ_h, in the columns AS-17 and AS-18 are 1.7% and 3%, respectively, while ρ_h of the columns tested by Lukkunaprasit and Sittipunt (2003) is in the order of 0.9% only. In addition, all of the longitudinal bars in the former columns are fully restrained by the transverse steel while those in the latter columns are not. Consequently, significant reduction in the compressive stress after buckling is predicted to occur for the columns with moderate confinement tested by Lukkunaprasit and Sittipunt (2003) while only slight reduction in compressive stress is predicted for the columns AS-17 and AS-18 with heavy confinement, as depicted in the stress-strain relationships of the longitudinal bars shown in Figure 4.8. In addition, as buckling occurs, the realistic confinement in core concrete is reduced due to excessive deformation of the concrete. This can cause further softening and hence reduction in the slope of the descending branch of the stress-strain relation of the core concrete which cannot be captured by the proposed confinement model. Thus, the realistic moment-curvature relationships of columns tested by Sheikh and Khoury (1993) cannot be predicted with satisfaction. It is obvious that further refinement in modeling buckling of longitudinal reinforcement as well as modeling of concrete under large axial strain is needed.

4.2 Cyclic Behavior of Reinforced Concrete Columns and Plane Frames

4.2.1 Finite Element Analysis

The finite element analysis program, FINITE (Lopez et al), was used in the analysis of reinforced concrete columns and plane frames in this study. FINITE was developed by the Civil Engineering department at the University of Illinois at Urbana-Champaign, the University of Kansas, the University of Wyoming and Carnegie-Mellon University. Nonlinear effects from strain-displacement relationships (geometrical nonlinearities) and from material constitutive relationships (material nonlinearities) are both included in the finite element formulation. Cracking of concrete is modeled by

means of the smeared crack procedure. The incremental-iterative Newton-Raphson algorithm is used for solving the nonlinear equilibrium equations.

4.2.2 Material Models for Finite Element Analysis

In order to investigate the behavior of reinforced concrete columns or plane frames using the finite element method, the nonlinear path-dependent constitutive models for both concrete and reinforcement are required. The important aspects of behavior in reinforced concrete member, which include tension stiffening, crack closing and reopening, compression softening, effects of confinement and strength degradation under cyclic loading should be considered in the formulation.

When concrete cracks, the concrete between cracks still carries tensile stress which is transferred through bond between the reinforcement and aggregate interlock in the surrounding concrete. Such behavior makes the average tensile stiffness of a reinforcement embedded in concrete greater than that of a plain reinforcement. This aspect is called tension stiffening. In Sittipunt and Wood (1993), the effect of tension stiffening is included in the concrete model as shown in Figure 4.9. In this model, tensile stress in concrete immediately drops from the cracking stress, σ_{cr}, to the smaller stress, $\alpha\sigma_{cr}$, after cracking. Then, as the tensile strain increases, the tensile stress decreases to a lower-bound stress, σ_i, at the tensile strain of ε_i.

Under cyclic loading, cracks close and reopen throughout the loading history. As the crack status changes from fully open to fully closed, the stiffness of cracked concrete increases from a value near zero to a value close to the initial modulus of elasticity of concrete. Schematic representation of crack closing and reopening is shown in Figure. 4.10. The typical compressive cyclic stress-strain relationship used in modeling the concrete is shown in Figure 4.11. Basic rules for defining such curve are based on the two curves: an envelope curve and a common point curve. The envelope curve defines the boundary of the permissible stress-strain coordinates and can be represented by the uniaxial stress-strain relationship of concrete under monotonic compression.

The shear stress function represents the relationship between the shear stress and the shear strain. The important aspects of the shear transfer mechanism that are included in the shear stress function are the interface shear stiffness, the dowel action stiffness and the loading and unloading rules for cyclic shear loadings. The shear stiffness of cracked concrete is composed of two components:

1. Shear stiffness from the aggregate interlock or the interface shear transfer, G_{ist}
2. Shear stiffness from dowel action, G_{dow}

The total shear stiffness, G can be written as follows:

$$G = G_{ist} + G_{dow} \tag{4.4}$$

The cyclic shear transfer model used is shown in Figure 4.12. As shown in Figure 4.12, the relationship between the shear stress, τ, and the shear strain, γ, consists of three regions: loading, unloading and slip. Details on these aspects are given in Sittipunt and Wood (1993).

Due to time constraint, only slight modification on the effects of confinement in FINITE could be made in this study. The confinement model proposed by Sheikh and Uzumeri (1982), originally incorporated in FINITE by Sittipunt and Wood (1993), does not include the influence of the flexibility of the perimeter ties. It was shown in the previous chapter that the flexibility of perimeter ties had profound influence on the confinement pressure at the peak confined compressive strength of core concrete. Therefore, the confinement model proposed by Sheikh and Uzumeri (1982) is replaced by the confinement model described in Chapter II. In modeling the cyclic behavior of the longitudinal bars, it was found that the original Ramberge-Osgood model in FINITE was not suitable to model the buckling behavior of the longitudinal reinforcement described in Chpater II. However, due to the problem in modeling the cyclic stress-strain relationship of the longitudinal reinforcements including buckling, the original Ramberge-Osgood model in the program FINITE is used to simulate the cyclic behavior of the longitudinal reinforcements without consideration of buckling.

4.2.3 Load-displacement Relationship for Reinforced Concrete Columns

The reinforced concrete column, CF135/0.30 described earlier was taken as a case study. The column was subjected to a cyclic lateral load under a constant axial force [Lukkunaprasit and Sittipunt (2003)]. The finite element mesh of the column is shown in Figure 4.13. The experimental load-displacement curve for column CF135/0.30 is shown in Figure 4.14 together with the analytical results obtained from the program FINITE. It can be seen from Figure 4.14 that, before the sudden drop of the load-carrying capacity, the predicted hysteretic loops agree quite well with the experimental results. However, the finite element model fails to predict the behavior of the column after the sudden degradation in the load carrying capacity. It was observed during the cyclic test of this column that some longitudinal bars started to buckle at this point. Due to the significant reduction in load carrying capacity of the buckled longitudinal bars, the load carrying capacity of the column is decreased significantly. Therefore, neglecting the influence of buckling in the finite element analysis results in unrealistic load-displacement relationship of the column at failure.

4.2.4 Load-displacement Relationship for Reinforced Concrete Plane Frames

A portal reinforced concrete plane frame subjected to cyclic loading is studied in this section. The details of cross-sectional configurations of columns and beam and the finite element model for half of the reinforced concrete frame are shown in Figures 4.15 and 4.16, respectively. The analytical load-displacement relationships of both frames from the program FINITE are shown in Figure 4.17. It can be seen from Figure 4.17 that the flexure dominated behavior with slight pinching effect is observed in both frames. Because Frame type I has a larger value of the volumetric ratio of the transverse steel, at the same lateral displacement, Frame type I can sustain a slightly larger value of lateral load than Frame type II, as expected. More importantly, the amount of confinement has significant influence on the maximum displacement capacity of the frames. During performing the finite element analysis of Frame II, the solutions fail to converge when a displacement greater than 35 mm. is applied to Frame II. Thus, as depicted in Figure 4.17, Frame I can sustain a maximum displacement of about 42 mm while Frame II can sustain only 35 mm. In addition, an increase in the pinching effect is observed for the reinforced concrete plane frame with a lower volumetric ratio of transverse steel in the column.

It is well known that modeling plane frames with 2-D plane stress elements results in a large number of elements which consumes much computational time for nonlinear analyses. Therefore, an alternative approach is explored in which highly nonlinear regions of the concrete members are modeled as 2-D plane stress elements while the remaining (essentially) elastic portions represented by elastic beams. A transfer beam assemblage embedded in the plastic hinge zone is employed at the plane stress-beam junction. Figure 4.18 shows Frame type II modeled as described, taking advantage of symmetry of the structure and anti-symmetry of the lateral loading. The properties of the transfer beam assemblage are selected such that the solution of the first hysteretic loop is close to that of the 2-D plane stress model. In this study, the moment of inertia of the transfer beams is taken to be equal to the moment of inertia of the gross section of the beam. The comparison of the analytical results from the current model with the previous one is shown in Figure 4.19. It is evident that, although the maximum difference between the analytical and experimental results at one yield displacement is about 10%, the solution of the simplified model fails to converge after the displacement reaches two times the yield displacement.

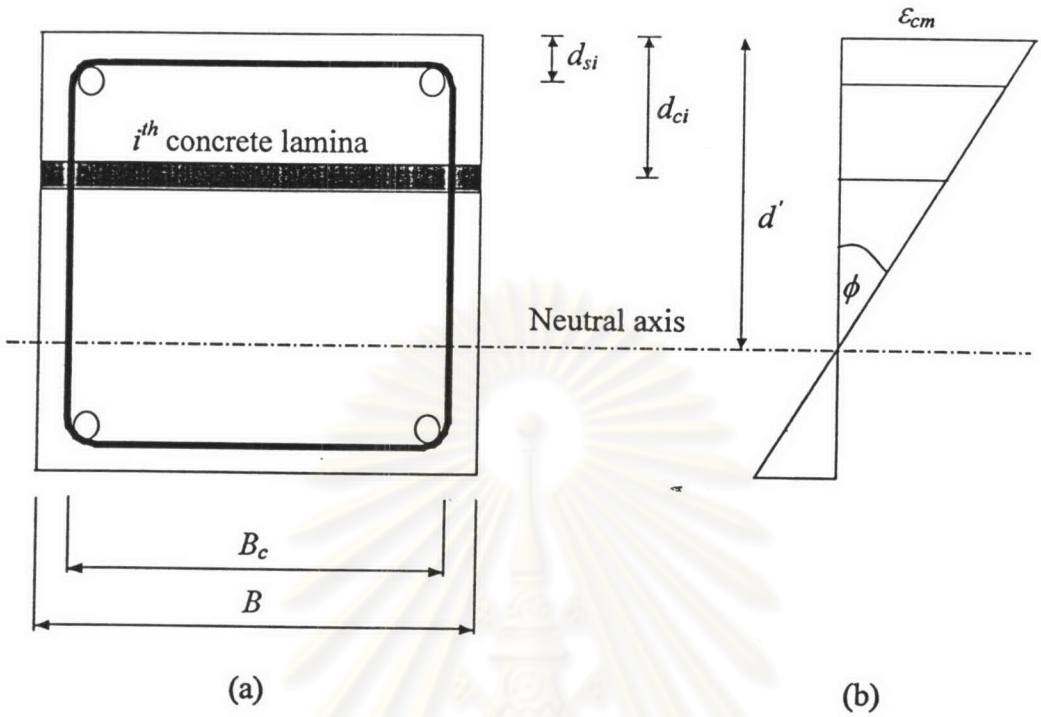

Figure 4.1 (a) Reinforced concrete column section (b) strain distribution

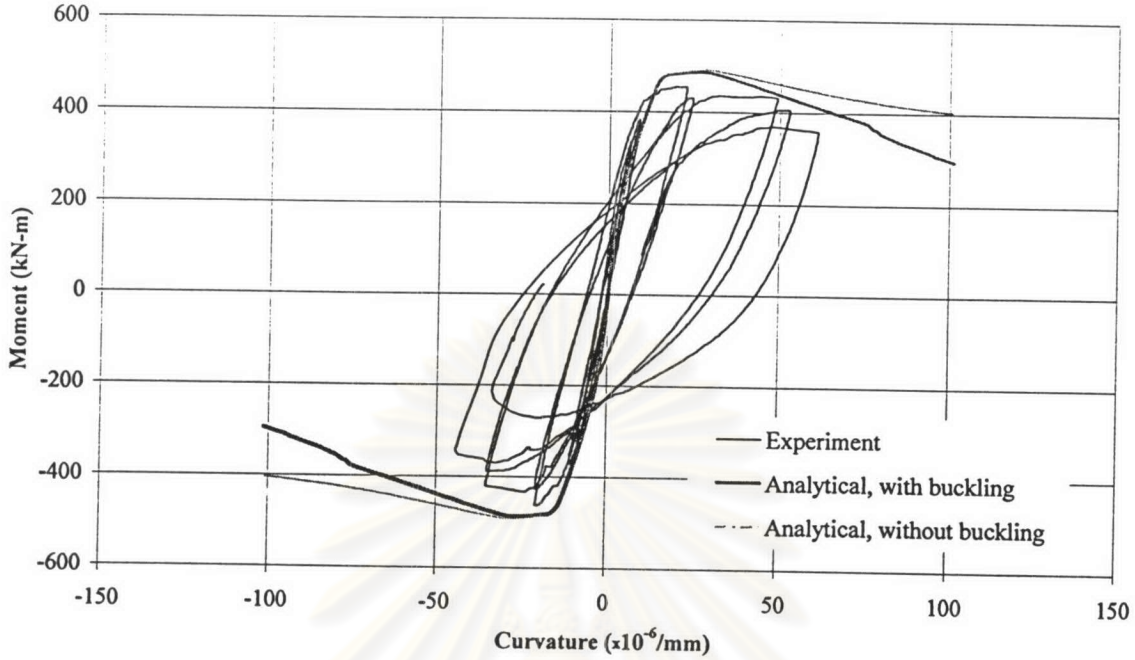

Figure 4.2 Comparison of predicted envelope moment-curvature relationship with experimental results for column CFL90/0.37

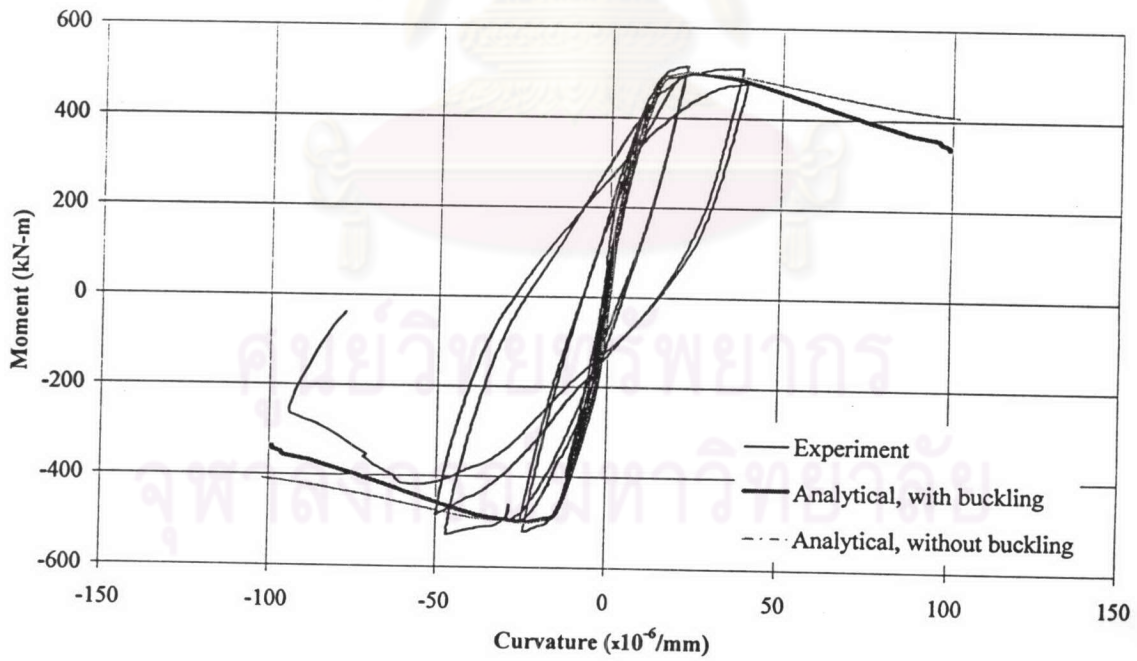

Figure 4.3 Comparison of predicted envelope moment-curvature relationship with experimental results for column CF135/0.30

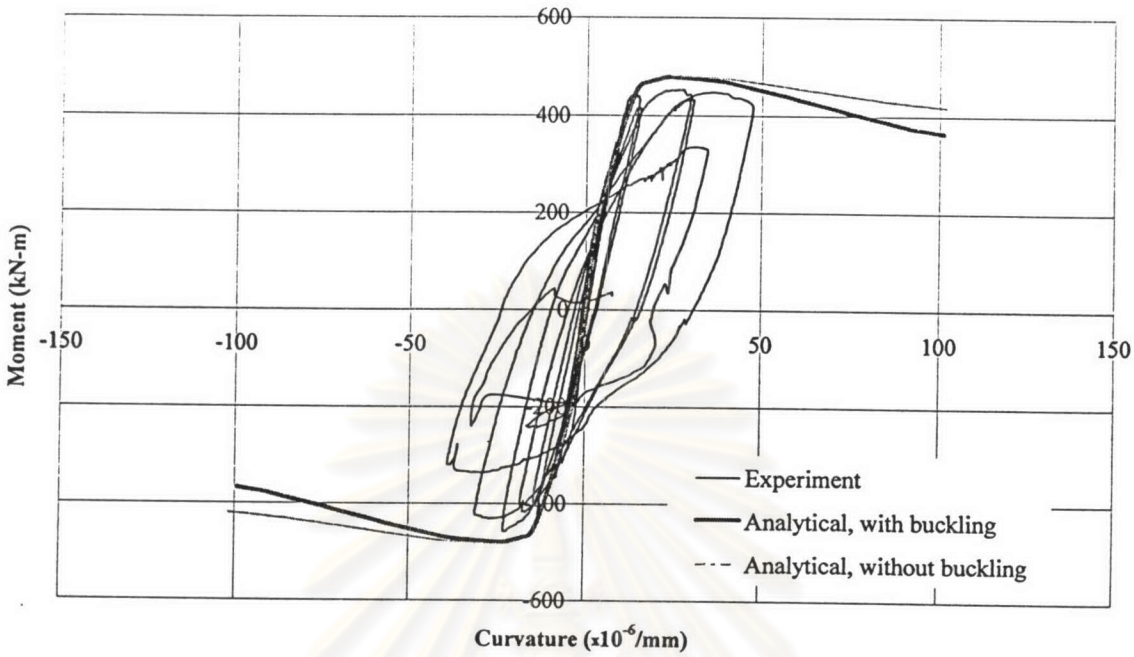

Figure 4.4 Comparison of predicted envelope moment-curvature relationship with experimental results for column CFL90/0.30

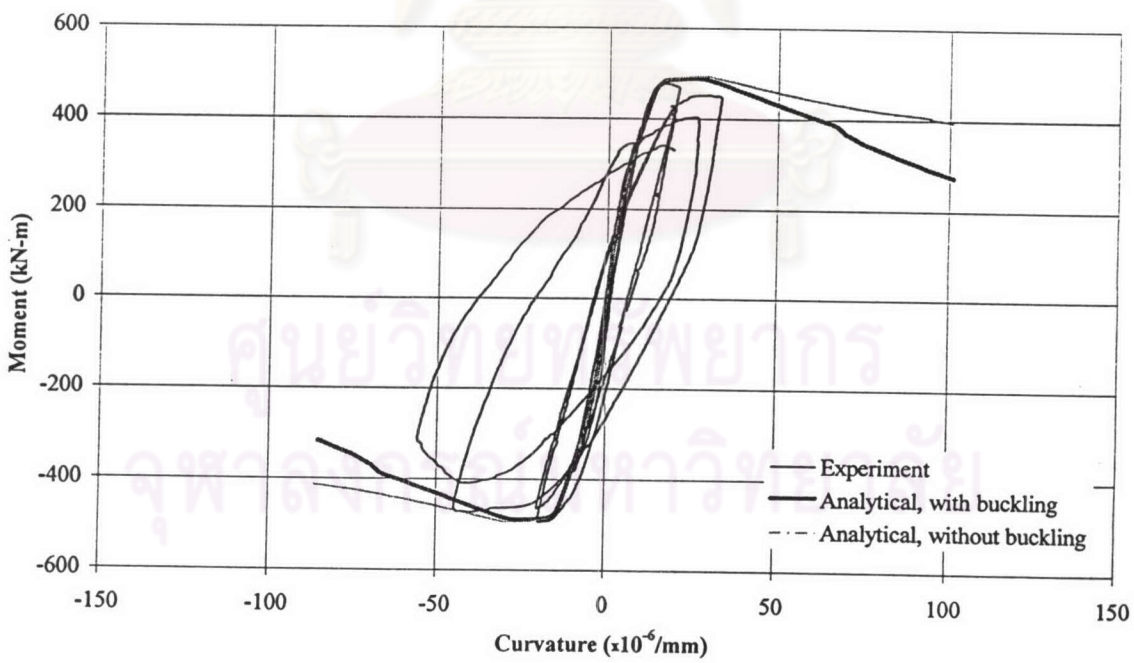

Figure 4.5 Comparison of predicted envelope moment-curvature relationship with experimental results for column CF135/0.37

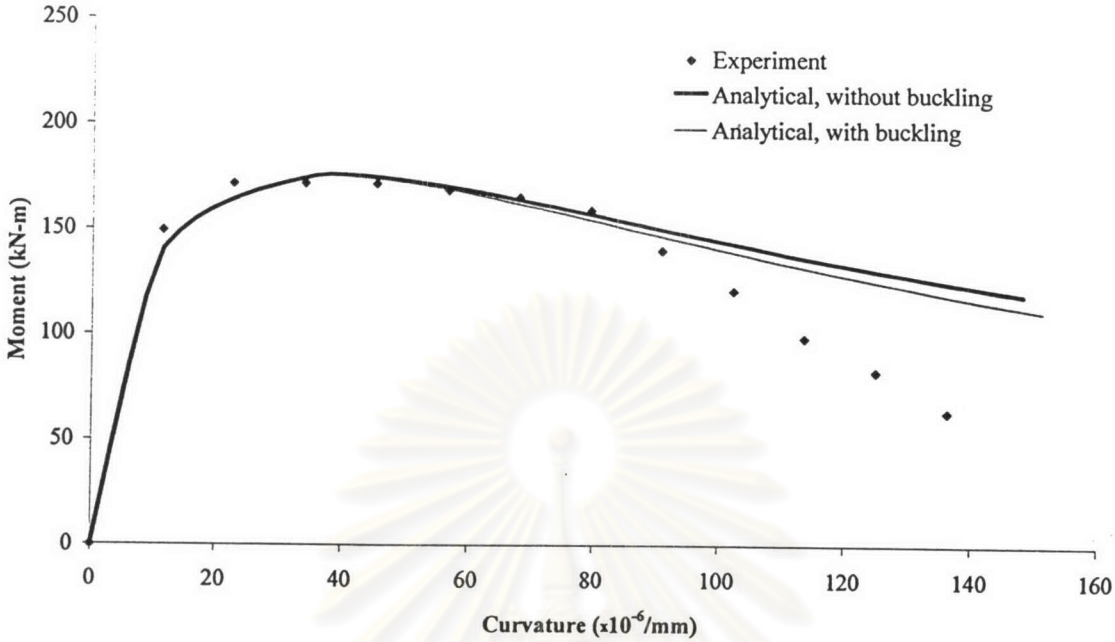

Figure 4.6 Comparison of predicted moment-curvature relationship with enveloped experimental results for column AS-17 [Sheikh and Khoury (1993)]

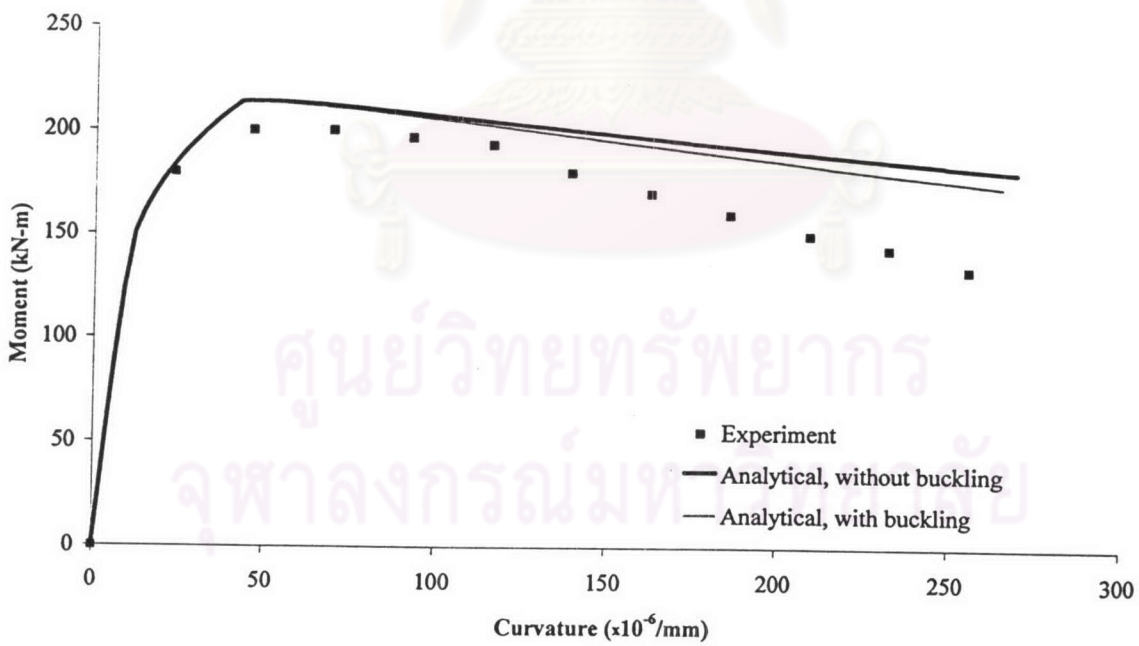

Figure 4.7 Comparison of predicted moment-curvature relationship with enveloped experimental results for column AS-18 [Sheikh and Khoury (1993)]

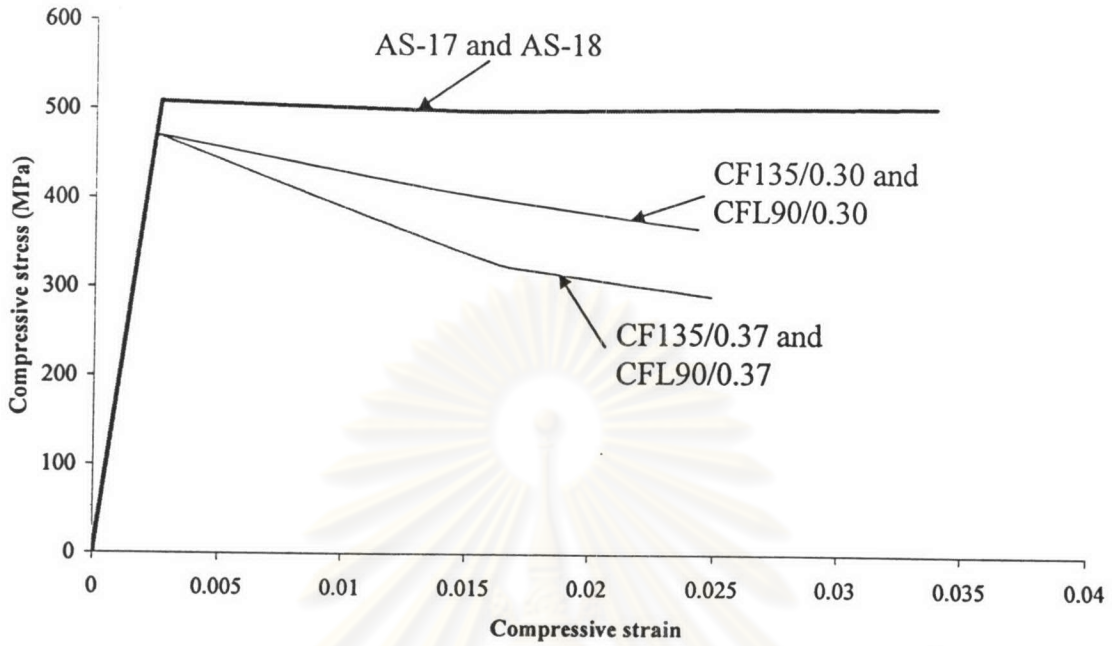

Figure 4.8 Analytical stress-strain relationships for longitudinal bars under compressive strain

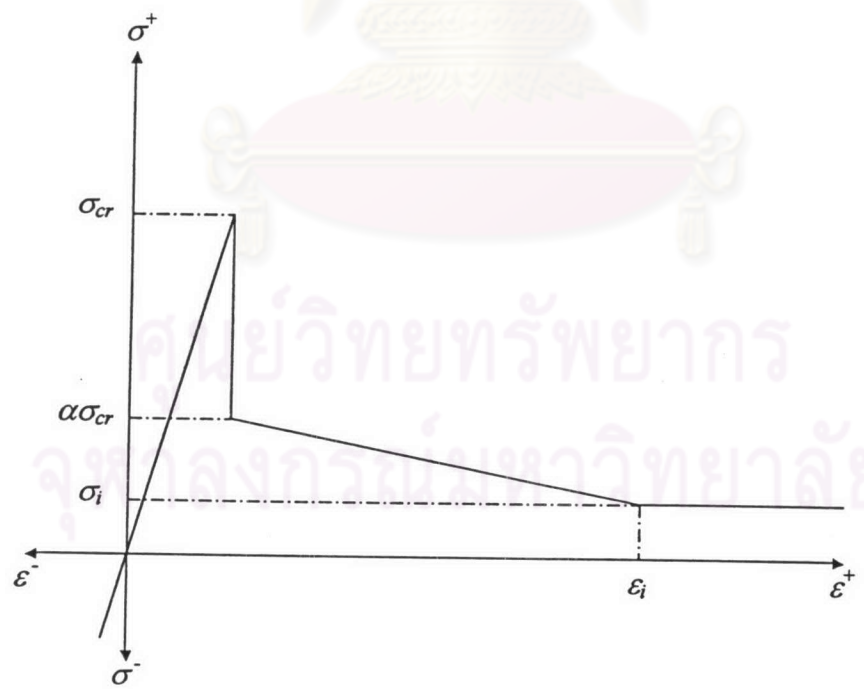

Figure 4.9 Tension stiffening model [Sittipunt and Wood (1993)]

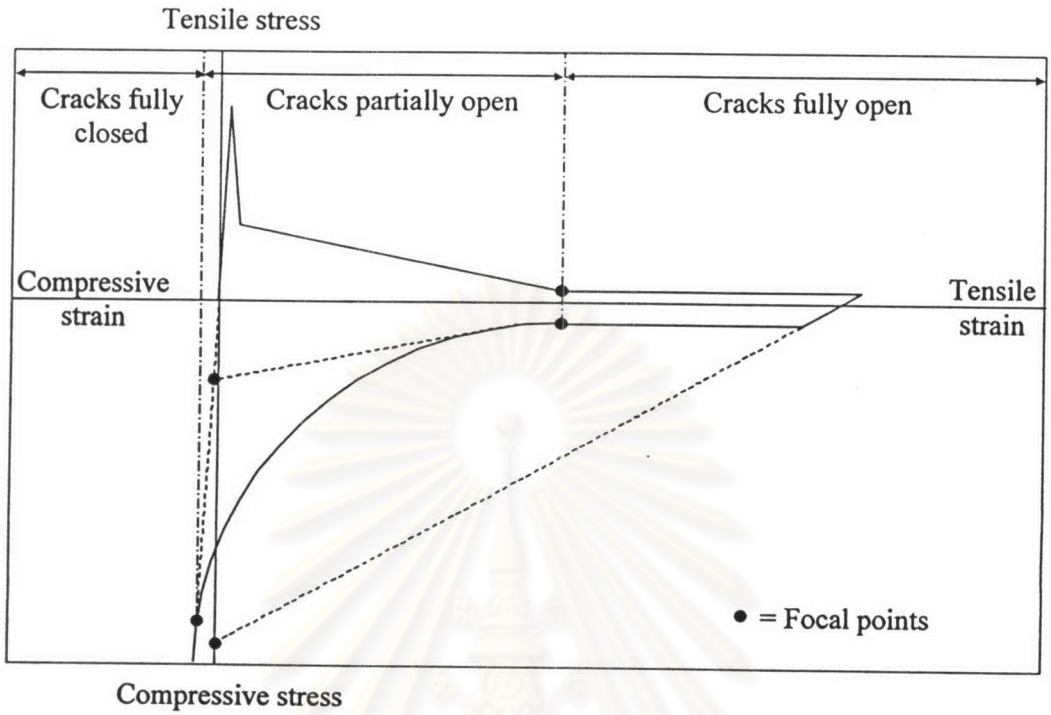

Figure 4.10 Schematic representation of crack closing and reopening in FINITE [Sittipunt and Wood (1993)]

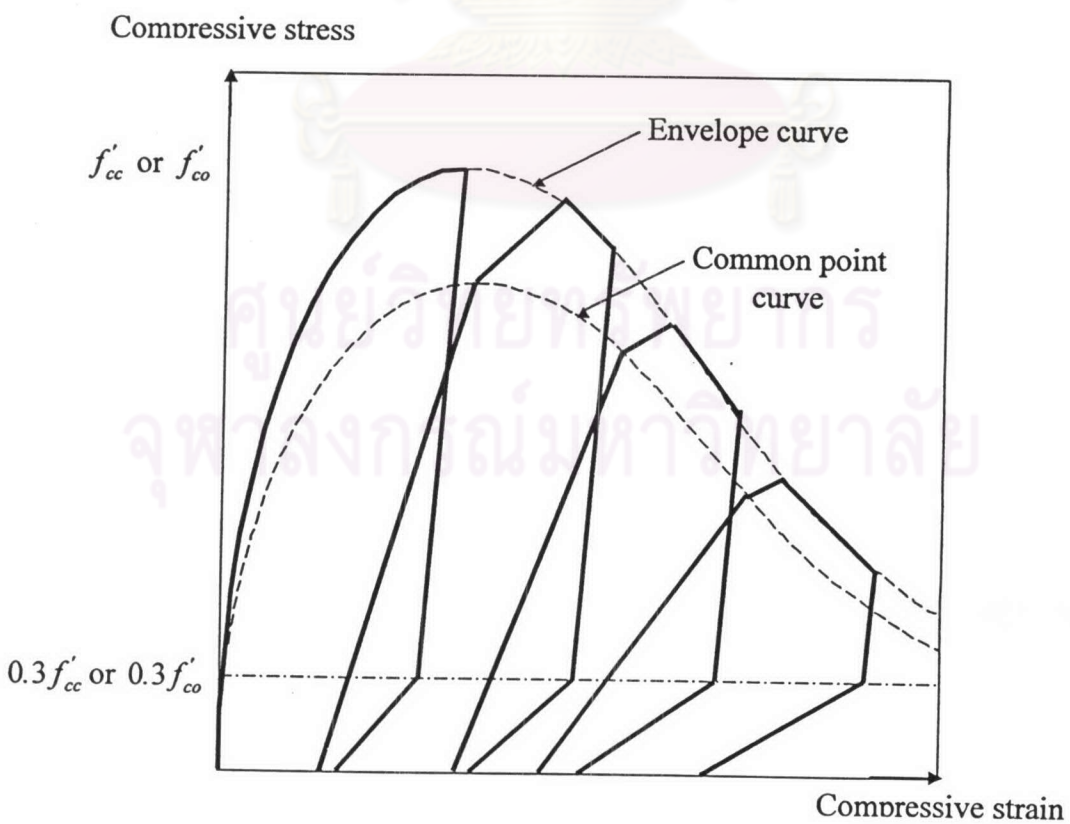

Figure 4.11 Compressive cyclic stress-strain relationship in FINITE [Sittipunt and Wood (1993)]

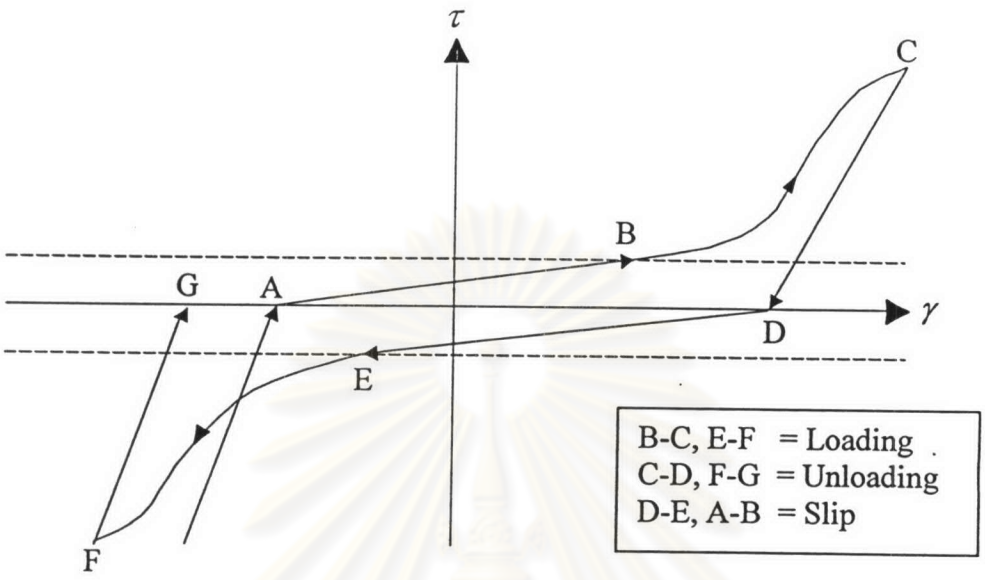

Figure 4.12 The cyclic shear model in FINITE

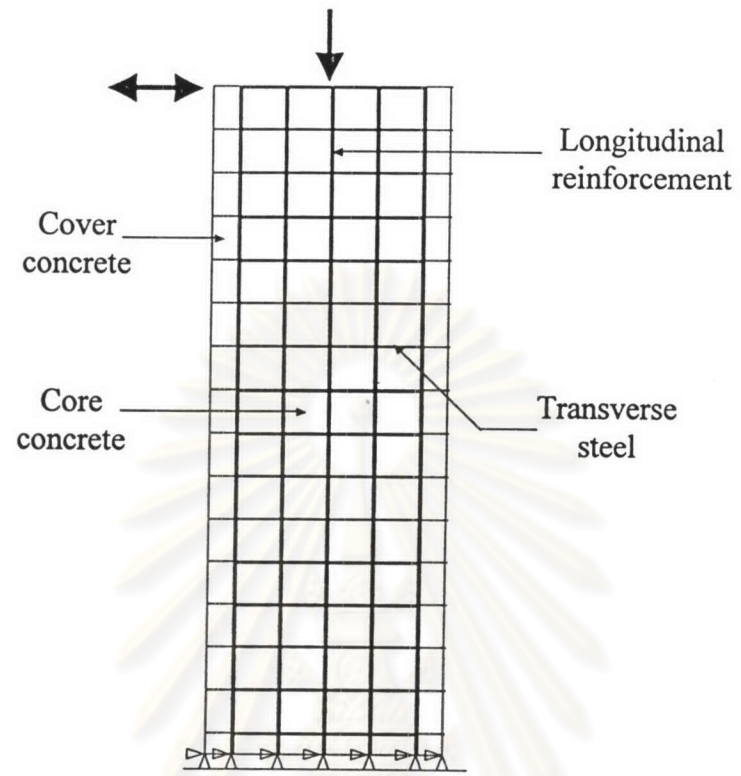

Figure 4.13 Finite element model for a reinforced concrete column

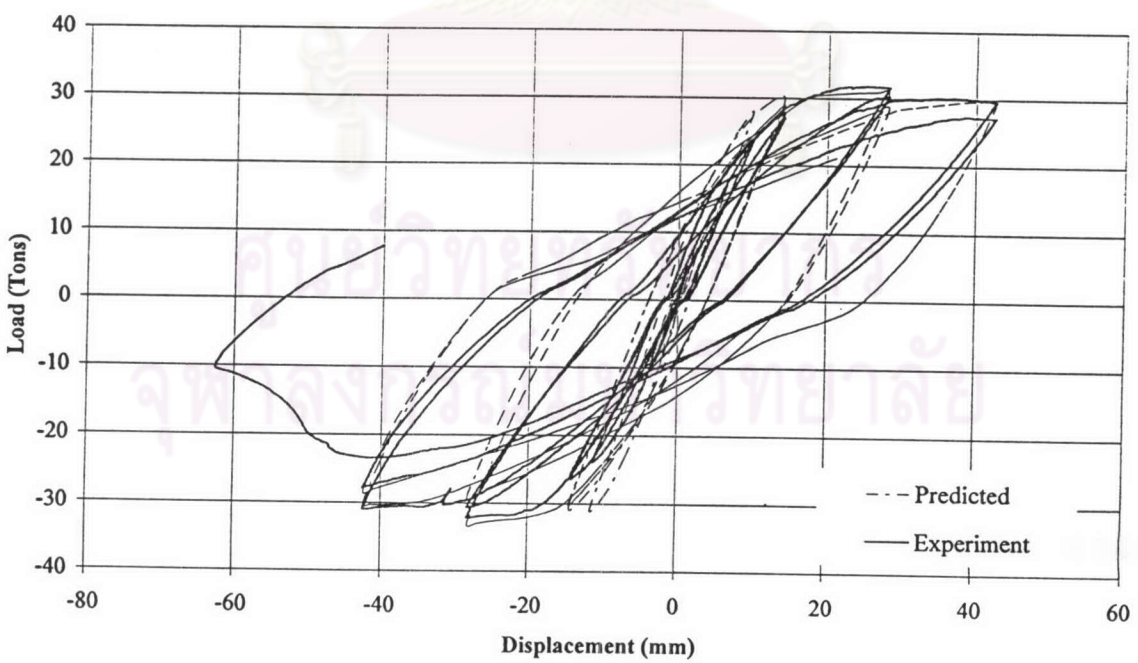

Figure 4.14 Comparison of experimental with analytical load-displacement curves for column CF135/0.30

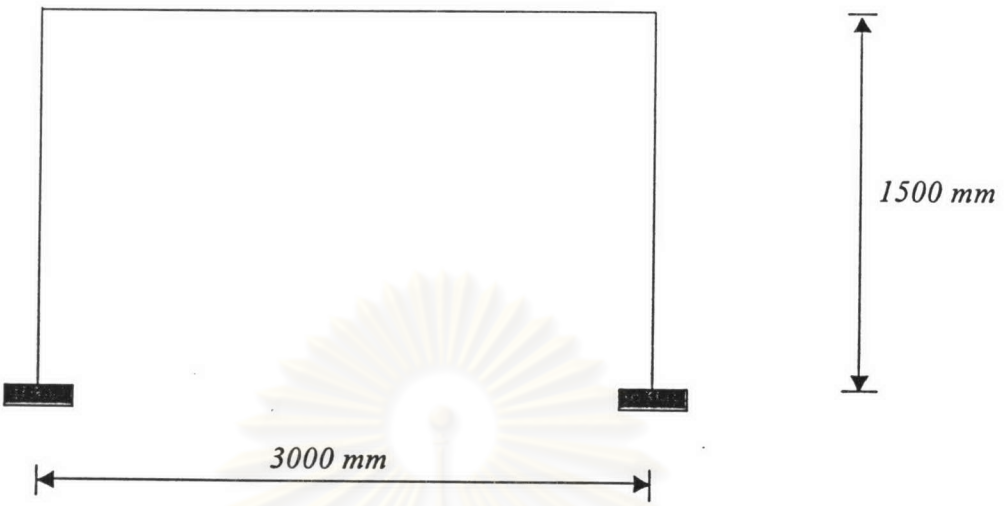

Frame I

	B (mm)	H (mm)	N_b	D (mm)	d_b (mm)	s (mm)
Column	250	250	4	16	9	75
Beam	150	300	4	16	6	75

Frame II

	B (mm)	H (mm)	N_b	D (mm)	d_b (mm)	s (mm)
Column	250	250	4	16	6	75
Beam	150	300	4	16	6	75

Figure 4.15 Dimensions and details for the RC plane frames (Frame I and II) used in the finite element study

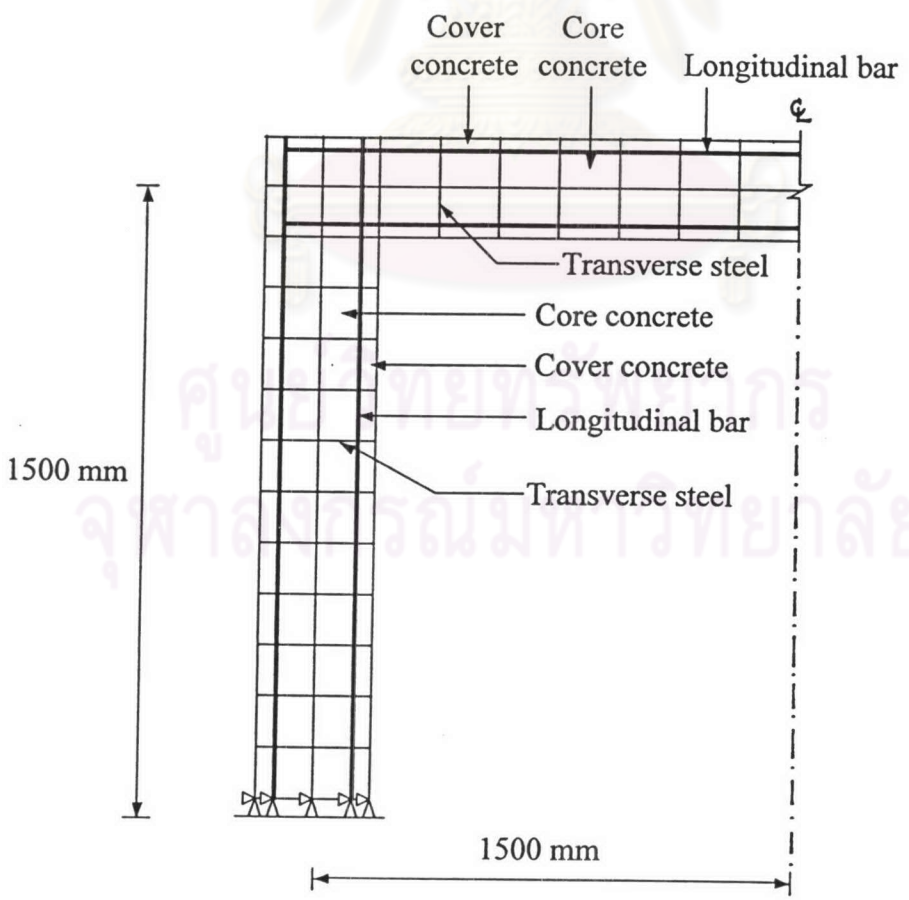

Figure 4.16 Finite element model for Frame type I and type II

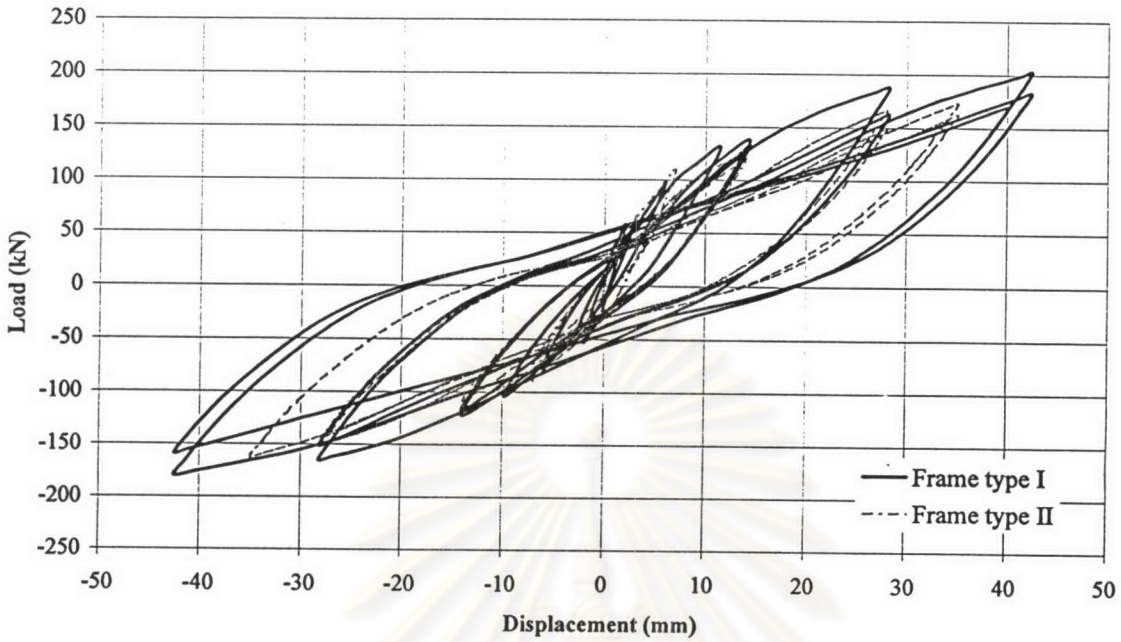

Figure 4.17 Load-displacement relationships for the Frame I and Frame II

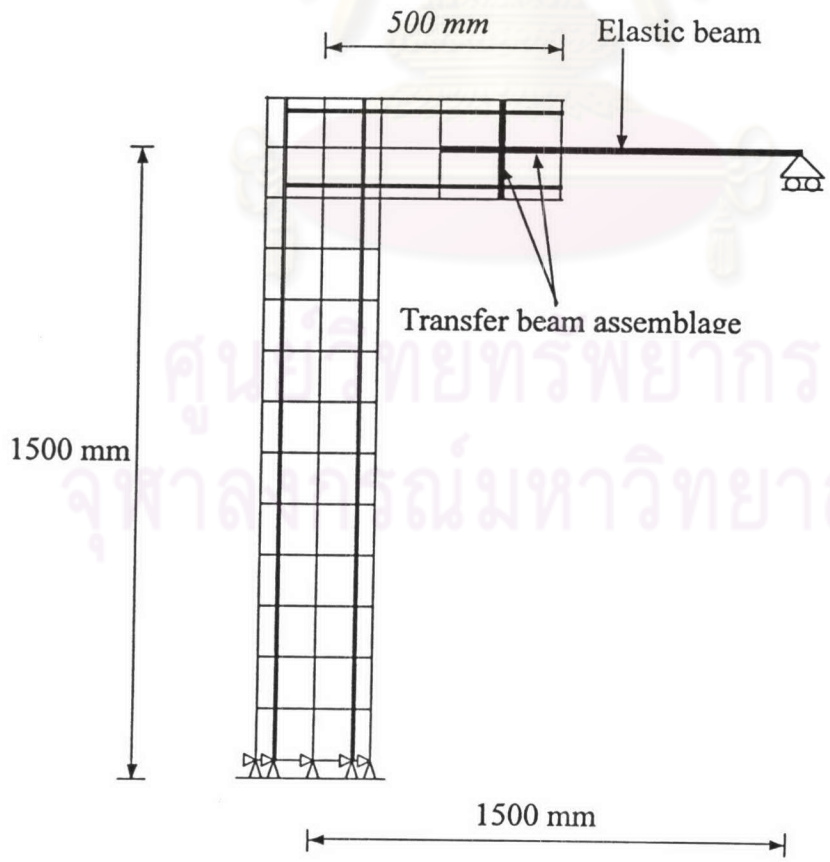

Figure 4.18 Simplified finite element model for Frame type II

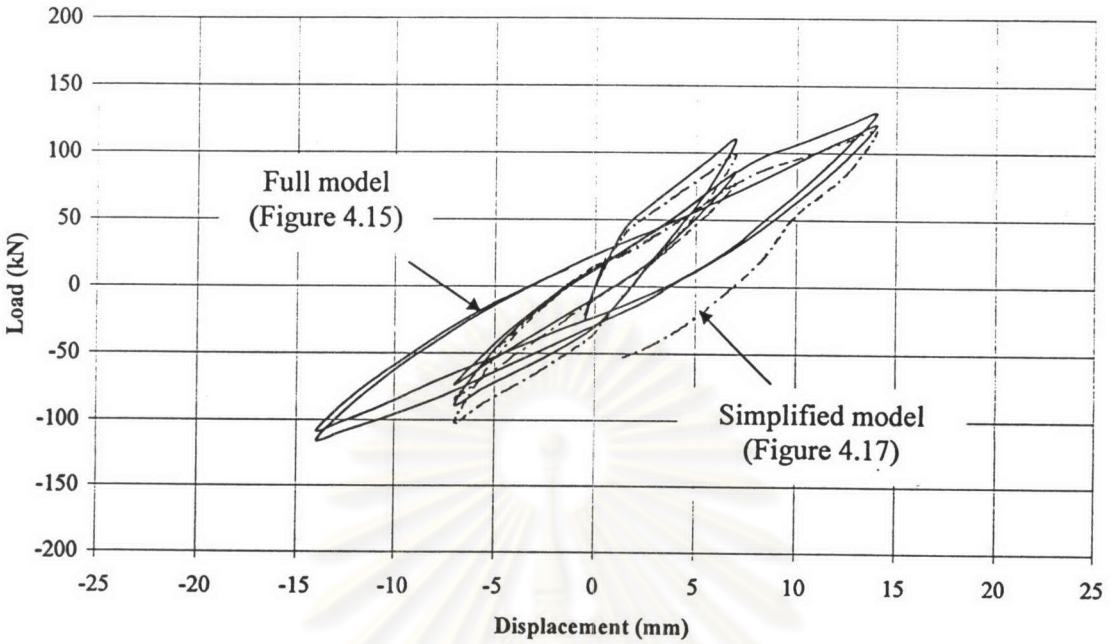

Figure 4.19 Comparison of solutions from full finite element model with simplified model

Table 4.1 Details of columns tested at Chulalongkorn University by Lukkunaprasit and Sittipunt (2003)

Column label (1)	ρ_t (%) (2)	Tie configuration (3)	B_c (mm) (4)	d_h (mm) (5)	s (mm) (6)	f_{yh} (MPa) (7)	f_{yl} (MPa) (8)	f_{co}' (MPa) (9)	f_{cc}' (MPa) (10)
CF135/0.30	0.88	Type 2	360	8.94	120.0	305	470	30.4	33.10
CF135/0.37	0.90	Type 2	360	9.08	120.0	318	475	25.9	27.70
CFL90/0.30	0.90	Type 2	360	9.06	120.0	306	470	26.9	29.83
CFL90/0.37	0.88	Type 2	360	9.00	120.0	304	470	27.5	30.37

Table 4.2 Details of columns tested by Sheikh and Khoury (1993)

Column label (1)	ρ_t (%) (2)	Tie configuration (3)	B_c (mm) (4)	d_h (mm) (5)	s (mm) (6)	f_{yh} (MPa) (7)	f_{yl} (MPa) (8)	f_{co}' (MPa) (9)	f_{cc}' (MPa) (10)
AS-17	1.68	Type 5	267	9.50	108.0	507	508	26.6	35.14
AS-18	3.06	Type 5	267	12.70	108.0	464	508	27.9	45.22